Chapter 4

# InP/InGaAS Symmetric Gain Optoelectronic Mixers

Wang Zhang and Nuri W. Emanetoglu

Additional information is available at the end of the chapter

http://dx.doi.org/10.5772/51461

## 1. Introduction

Optoelectronic mixers (OEM) are photodetectors which detect an optical signal and internally mix it with an electrical signal to obtain an electrical base-band (low frequency) signal. OEM devices have applications in optical communications and sensors such as laser assisted detection and ranging (LADAR) systems. Optoelectronic mixers can simplify signal processing in an optoelectronic system by combining the photodetection and mixing functions, leading to reduced component count. An optoelectronic mixing device which also amplifies the detected signal would further benefit the system.

In this work, a symmetric gain optoelectronic mixer based on a lattice-matched indium gallium arsenide ($In_{0.53}Ga_{0.47}As$) / indium phosphide (InP) symmetric heterojunction phototransistor structure is investigated for chirped-AM laser detection and ranging systems (LADAR) operating in the "eye-safe" 1.55 μm wavelength range. The symmetric current-voltage (I-V) characteristics of this device allows for it to be operated without the application of a DC bias voltage.

### 1.1. LADAR and the need for optoelectronic mixing devices

The requirements and constraints of the application, LADAR, determine the specifications of the SG-OEM device. Therefore, a basic review of the application is necessary.

Two types of LADAR systems exist, pulse and continuous wave systems, both of which operate in similar manner to their RADAR equivalents [1]. In pulsed LADAR, a laser pulse is transmitted, and the time-of-flight of the return signal is measured. The alternative is to modulate the intensity of a continuous-wave laser with a chirped-FM signal. In order to avoid confusion with optical wavelength modulation, this method has also been called chirped-AM LADAR [2]. The frequency difference ($f_{IF}$) between the reference (LO) and return (RF) signals is related to target distance by:

$$f_{IF} = 2\Delta F \frac{D}{cT} \quad (1)$$

where ΔF the difference between the start and end frequencies of the chirp, T the chirp period, c the speed of light and D the distance to target. The chirp may cover frequencies ranging from hundreds of MHz to several GHz. In contrast, the mixing product is in the range of tens of kHz to several MHz, as a function of the chirp period T and distance D.

The primary advantage of chirped LADAR over pulsed LADAR is the ability to use semiconductor lasers as the transmitter source, leading to lower cost, power and weight. An additional advantage for a LADAR-on-chip implementation is that by using an optoelectronic mixer device, as described below, the microwave bandwidth return signal can be converted into a low frequency electrical signal that can be read-out using CMOS technology.

A typical photodetector in an optoelectronic system would be DC biased, and convert the RF modulation of the optical signal to an electrical signal at the RF frequency. In a chirped-AM LADAR system this RF signal output is then electronically mixed with LO signal. Due to the small available optical power, below 1 nW in some applications, the RF signal output of the detector may need to be amplified with a wide band amplifier before the electronic mixing. This amplifier can only have a low gain, due to the wide bandwidth nature of the RF signal. An alternative is to mix the photodetector output with the LO signal, then amplify the low frequency signal.

Signal processing of a chirped-AM LADAR system is simplified if the photodetector is used as an optoelectronic mixer (OEM) [2]. An optoelectronic mixer is a photodetectorwhose responsivity is modulated with the LO signal. The OEM output contains the difference (IF), sum, LO and RF signals. The mixed output signal is low-pass filtered to isolate the IF signal, which is then amplified. Due to the frequency difference, tens to hundreds of kHz vs. hundreds of MHz, much higher gains are possible in the following transimpedance amplifier.

A symmetric I-V characteristic photodetector can be used as an optoelectronic mixer. Symmetric I-V characteristics refer to having equal absolute magnitude current for equal absolute magnitude voltage, I(-V) = -I(V), with I(0) = 0. This allows driving the OEM directly with the LO signal, without a DC bias. The output of the detector will thus contain the LO, RF, IF and sum frequencies. This output can be low pass filtered and the IF signal amplified. As this IF signal's bandwidth can be up to six orders of magnitudes smaller than the carrier frequencies, much higher gains can be used at the trans-impedance amplifier (TZA) following the OEM. Due to the lack of a DC bias, sensitivity to background light is reduced, as the response from background light averages to zero. An additional 3 dB signal processing gain is also obtained. The metal-semiconductor-metal (MSM) Schottky photodetector is such a symmetric device [2-5]. Chirped-FM LADAR with GaAs MSM optoelectronic mixers, operating in the 800-850 nm wavelength range, have been reported [2,3]. Eye-safe operation requires operating wavelengths in the 1.3 μm to 1.55 μm. This has motivated to development of InGaAs MSM optoelectronic mixers for operation at 1550 nm [4,5]. These InGaAs MSMs have been reported to have dark currents two orders of magnitude larger than GaAs MSMs [5], affecting noise level, and require larger RF power to achieve similar performance to GaAs

http://dx.doi.org/10.5772/51461

MSMs. The DC responsivity of the InGaAs MSM optoelectronic mixers was reported to be approximately 0.34 A/W [4,5].

The symmetric MSM Schottky photodetectors do not have a gain mechanism. Incorporating gain to the optoelectronic mixer would allow the following transimpedance amplifier's gain to be reduced, increasing bandwidth and improving the system's noise performance.

### 1.2. Phototransistors as optoelectronic mixing devices

There are three possible candidate structures, based on the avalanche photodiode (APD), the heterojunction phototransistor (HPT) and the modulated barrier diode (MBD). The avalanche photodiode suffers from several drawbacks, including excess noise, and high sensitivity to temperature, voltage bias and defects in the semiconductor material. HPTs and MBDs, on the other hand, can provide high gain with low noise. The basic HPT and MBD structures are shown in Figure 1. MBDs in particular are low noise devices, which have higher gain for lower incident optical powers. A standard asymmetric heterojunction HPT or MBD requires a DC bias to achieve the associated high gain. In a typical system, the DC biased device is used to detect the incoming optical signal at RF frequency. This signal may need to be amplified electronically. However, only low gains are possible due to the frequency. The next stage employs a mixer circuit to obtain the IF signal from the difference of the RF and LO signals. The IF signal may need further amplification.

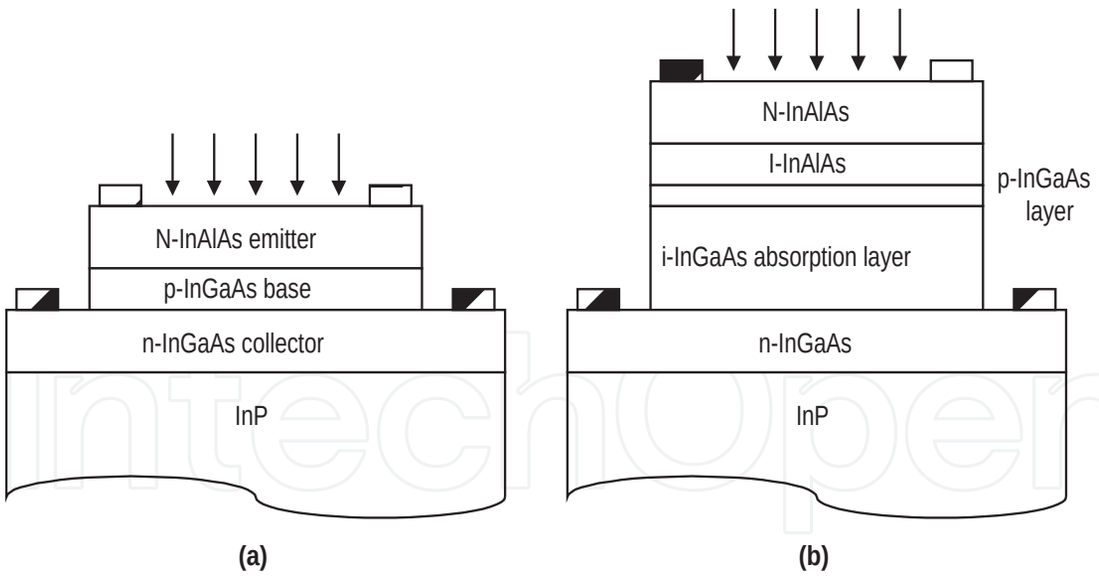


**Figure 1.** Basic structures of (a)heterojunction phototransistor; and (b) modulated barrier diode.

The heterojunction phototransistor is a transistor with its emitter made of a wider bandgap material than the base. This improves carrier injection efficiency, and also ensures absorption is limited to the base and the base-collector depletion region. The basic HPT is a two terminal device. A number of modifications to the basic HPT structure have been investigated to improve performance. A base bias can be provided, either optically or by an electrical

contact [6]. The base composition can be graded to establish an electric field which enhances electron transport [7,8].It was demonstrated that symmetric-area heterojunction phototransistors have a larger bandwidth than asymmetric area HPTs [9]. It should be noted that while Milano *et al* predicted a rather pessimistic bandwidth, improvements in material growth, device design and fabrication techniques have improved the maximum bandwidth of HPTs to the tens of GHz range [10,11].

HPT responsivity typically increases with increasing optical power. This has been attributed to recombination at the base-emitter heterojunction.It is desirable to have gain independent from the optical power, or have larger gain at lower optical power levels. Leu *et al* have demonstrated an approach to improve the gain dependence on optical power, by adjusting the doping profile of the emitter and base layers of InP emitter/InGaAs base HPTs [12]. By using a high-low emitter doping, that is reducing the emitter doping in a thin layer at the emitter-base junction, they eliminated the quantum well trapping the electrons at this interface. Thus, the recombination currents were reduced, and the ideality factor of the transistor improved, leading to a flattening of the gain vs. incident power characteristics.

HPTs have been demonstrated for optoelectronic mixing applications, where the LO signal was provided electrically [10,13] or optically [14].

The modulated barrier diode, also known as the Camel diode, is a non-Schottky majority carrier diode in which the carrier transport is controlled by a potential barrier in the bulk of the semiconductor. The application of MBDs as photodetectors was first demonstrated by A.Y. Cho and co-workers [15,16], who also showed its application in a picosecond sampling system [17]. The gain of the MBD is due to the hole trapping at the heterostructure interface. As holes accumulate in this quantum well, the barrier height will be lowered, resulting in an increased electron current, thus providing gain. As a majority carrier device, the MBD has fast intrinsic response [15,17]. In contrast with the HPT, the MBD device has higher responsivity at lower optical power levels [15,16]. The MBD has been used in a front-end photoreceiver, integrated with an FET [18], and a monolithically integrated phototransceiver in which it was integrated with an LED [19]. In the first case, the MBD and FET shared a common structure, and circuit utilized the MBD's gain and response speed. In the second case, the MBD's increasing gain with lower optical power was utilized to improve optical transceiver performance.

### 1.3. Symmetric gain optoelectronic mixers

Symmetric Gain OptoElectronic Mixers (SG-OEMs) for chirped-AM LADAR operating in the "eye-safe" 1.55 μm wavelength have been investigated by our research group at the University of Maine. These devices are based on symmetric heterojunction phototransistors.

The first generation SG-OEMs used indium aluminum arsenide ($In_{0.52}Al_{0.48}As$)/ indium gallium arsenide ($In_{0.53}Ga_{0.47}As$) heterostructures grown on InP substrates [20,21].The device structures were designed and simulated using the TCAD-Sentaurus tools from Synopys. These simulations prediced mixing responsivities up to 100 A/W for these devices.

http://dx.doi.org/10.5772/51461

The heterostructures were grown using molecular beam epitaxy at the US Army Research Laboratory, Adelphi, MD. Cracking defects in the thin films were revealed during device fabrication, leading to an investigation into an alternative device structure with indium phosphide (InP) layers to improve the growth quality [22,23].

## 2. Device Structure and Simulation

A schematic of the InP based symmetric gain optoelectronic mixer is shown in Figure 2. The targeted operating wavelength is 1.55 μm, therefore the base is $In_{0.53}Ga_{0.47}As$, which has a bandgap of approximately 0.74eV at 300K and is lattice matched to the InP substrate. The base is doped with acceptor atoms to obtain a p-type region. The n-type emitter/collector layers in the structure are made of InP. Highly doped n-type InP/$In_{0.53}Ga_{0.47}As$ layers are used for ohmic contact formation with the metal electrodes. The schematic in Figure 2 also shows highly doped interface layers at the emitter-base and collector-base interfaces. The device, as shown, is configured for top illumination.

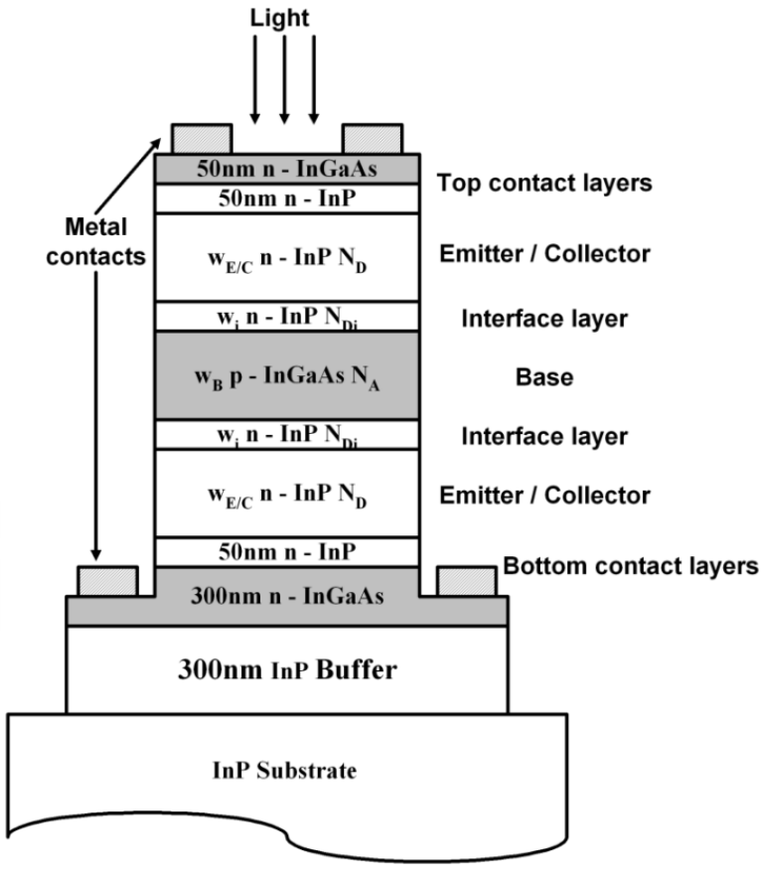


**Figure 2.** Schematic of an InP/ InGaAs symmetric gain optoelectronic mixer, top illumination configuration.

The design parameters investigated in this work are the base and emitter/collector layer thicknesses and doping levels, as identified in Table 1. The base width $w_B$ is the primary pa-

rameter that will determine the responsivity of the optoelectronic mixer. Increasing the base thickness will extend the carrier path and decrease transistor gain. This will lead to a decrease in the dark and optical currents. However, a trade off has to be made between light absorption, which is directly proportional to base thickness, and the recombination of light generated carriers in the base, which is inversely proportional to base thickness. The responsivity, R, is proportional to:

$$R \propto \frac{\left(1 - e^{-\alpha w_B}\right)}{d^2} \tag{2}$$

where $w_B$ is the thickness of the base region and $\alpha$ is the absorption coefficient. The base thickness and doping will also impact the base narrowing due to the growth of the reverse biased collector-base junction depletion region with increasing reverse bias, known as the Early effect. When the device is sufficiently reverse biased, the collector-base depletion region will reach the base-emitter depletion region, shorting the device. This is known as punch-through breakdown, and should be avoided.

| Symbol | Parameter |
|---|---|
| $w_B$ | $In_{0.53}Ga_{0.47}As$ base thickness |
| $N_A$ | $In_{0.53}Ga_{0.47}As$ base acceptor doping density, p-type |
| $w_{E/C}$ | InP emitter/collector thickness |
| $N_D$ | InP emitter/collector donor doping density, n-type |
| $w_i$ | InP emitter/collector-base interface layer thickness |
| $N_{Di}$ | InP emitter/collector-base interface layer donor doping density, n-type |

**Table 1.** Design parameters investigated for the symmetric gain optoelectronic mixer

Emitter/collector doping impact device performance in several ways. If they are highly doped, most of the depletion region will be in the base, significantly reducing the effective base thickness. This will provide higher transistor gain, but will also result in punch through breakdown of the device at low voltages. If these layers are lightly doped, then the series resistance will increase, reducing the available current from the device. The effect of the interface layers on device performance are also investigated in this work.

The work reported here covers device design, simulation and optimization using the 2D/3D TCAD-Sentaurus device simulator package from Synopsys, and device modeling. Parameters investigated for device optimization include the highly doped emitter-base interface layers, the base thickness and the doping of each layer. The horizontal dimensions of the standard device are summarized in Table 2. The simulation results are discussed in section 3 and the device model is presented in section 4.

http://dx.doi.org/10.5772/51461

| Parameter | Size [μm] |
|---|---|
| Inner mesa width | 16 |
| Outer mesa width | 30 |
| Top contact window width | 12 |
| Top contact metal width | 14 |
| Bottom contact window width | 2 |
| Bottom contact metal width | 4 |

**Table 2.** SG-OEM horizontal dimensions

## 3. DC Simulations: Dark Current and Responsivity

### 3.1. Comparison of InAlAs/InGaAs and InP/InGaAs SG-OEMs

The switch to InP layers was proposed due to the film stoichiometry and resulting lattice mismatch issues experienced with InAlAs films [20]. The first task in this project was to determine how the switch to InP would impact predicted device performance. Figure 3 compares the simulated I-V characteristics for two structures based on Figure 2. The layer thicknesses and doping densities are given in Table 3. InP_A is the structure shown in the figure, while in InAlAs_A all of the InP film layers are replaced by InAlAs, as reported in [20,21]. Both the dark current (i.e., no incident light) and the current with an incident optical power density of 1 mW/cm$^2$ are displayed. The light is set to be incident on the device's inner mesa and has the same width, 16μm. A transparent electrode was assumed. The incident optical power on the detector is 160 pW/μm. The figure illustrates the behavior of a device for a bias voltage sweep from 0 V to 5V.

| Parameter | Value |
|---|---|
| $w_B$ | 800 nm |
| $N_A$ | $2.5x10^{16}$ cm$^{-3}$ |
| $w_{E/C}$ | 390 nm |
| $N_D$ | $1x10^{16}$ cm$^{-3}$ |
| $w_i$ | 10 nm |
| $N_{Di}$ | $5x10^{-18}$ cm$^{-3}$ |

**Table 3.** Layer thickness and doping values for the simulations presented in Figure 3.

The simulation predicts that the $In_{0.52}Al_{0.48}As$/ $In_{0.53}Ga_{0.47}As$ based device will have larger dark and optical currents than the InP/ $In_{0.53}Ga_{0.47}As$ one over the bias range. The optical current of the $In_{0.52}Al_{0.48}As$/ $In_{0.53}Ga_{0.47}As$ based structure is 2.19 nA/μm at 2 V, compared to 1.64

nA/μm at 2 V for the InP/ $In_{0.53}Ga_{0.47}As$ based structure. The dark current is also larger for the InAlAs based device. This latter result initially seems counter-intuitive, as $In_{0.52}Al_{0.48}As$ has a larger bandgap than InP, as indicated in Table 4. Table 4 lists the material parameters for the three semiconductor materials, as calculated by TCAD Sentaurus for these compositions at 300K. This behavior can be attributed to two separate mechanisms. First, InP and InAlAs have different conduction band offsets with InGaAs. Second, the Early effect, i.e. base narrowing, is more prominent in the InAlAs based devices.

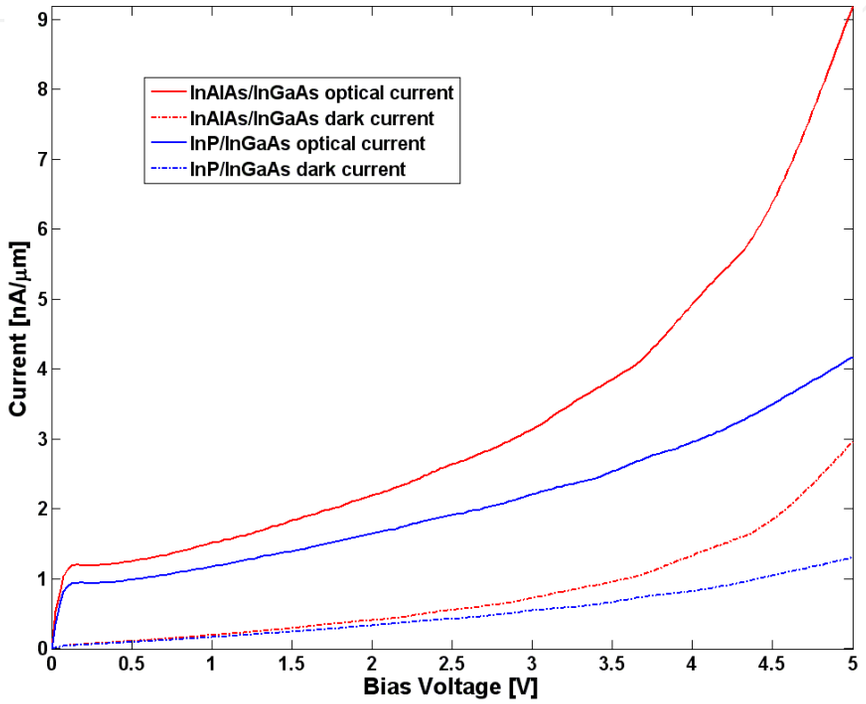


**Figure 3.** Dark and optical currents versus bias voltage for InP/ $In_{0.53}Ga_{0.47}As$ and $In_{0.52}Al_{0.48}As$/ $In_{0.53}Ga_{0.47}As$ based symmetric gain optoelectronic mixers with the same layer thickness and doping.

| | $In_{0.53}Ga_{0.47}As$ | InP | $In_{0.52}Al_{0.48}As$ |
|---|---|---|---|
| $E_g$ [eV] | 0.718721 | 1.33587 | 1.48159 |
| $\chi_0$ [eV] | 4.5472 | 4.4 | 4.2711 |
| $\varepsilon_r$ | 13.9061 | 12.4 | 12.3948 |
| $N_c$ [$cm^{-3}$] | $2.5396x10^{17}$ | $5.66x10^{17}$ | $5.7814x10^{17}$ |
| $N_v$ [$cm^{-3}$] | $7.5107x10^{18}$ | $2.03x10^{19}$ | $9.4152x10^{18}$ |

**Table 4.** Material parameters used by TCAD Sentaurus in the device simulations

The different conduction band offsets results in a significantly larger two-dimensional electron gas (2DEG) concentration at the InGaAs side of the InP/InGaAs contact layer $n^{++}$-$N^{++}$

http://dx.doi.org/10.5772/51461

isotype heterojunction compared to that in the InAlAs/InGaAs case, as predicted by TCAD Sentaurus simulations. The electron concentrations at this interface for both structures is shown in Figure 4. The InP based device is on the left, and the InAlAs based device is on the right. The top layer (above the line at 2.3 μm) is the InGaAs contact layer, and below it is the wider bandgap layer. In the InP/InGaAs structure, the 2DEG induces a depletion layer on either side of it (denoted by the white lines), about 7.5 nm in total, larger than that in the InAlAs based device, which is about 2 nm.

Base width narrowing also contributes to the larger InAlAs/InGaAs SG-OEM current. The effective base width is defined as:

$$x_B = w_B - x_{df} - x_{dr} \tag{3}$$

where $x_B$ is the effective base width, $x_{df}$ is the depletion region width of the forward biased heterojunction and $x_{dr}$ is the depletion region width of the reverse biased heterojunction. The change of the forward biased junction width due to the bias voltage is relatively small compared to the reverse biased junction, and can be considered to be its 0V bias value. From TCAD Sentaurus simulations, the effective base width at 1V for the InP based structure is predicted to be 719.17 nm, and 710.19 nm for the InAlAs based structure. Considering the magnitude of this difference, it can be concluded that the dominant reason for the smaller dark current in the InP based devices is the conduction band edge discontinuity.

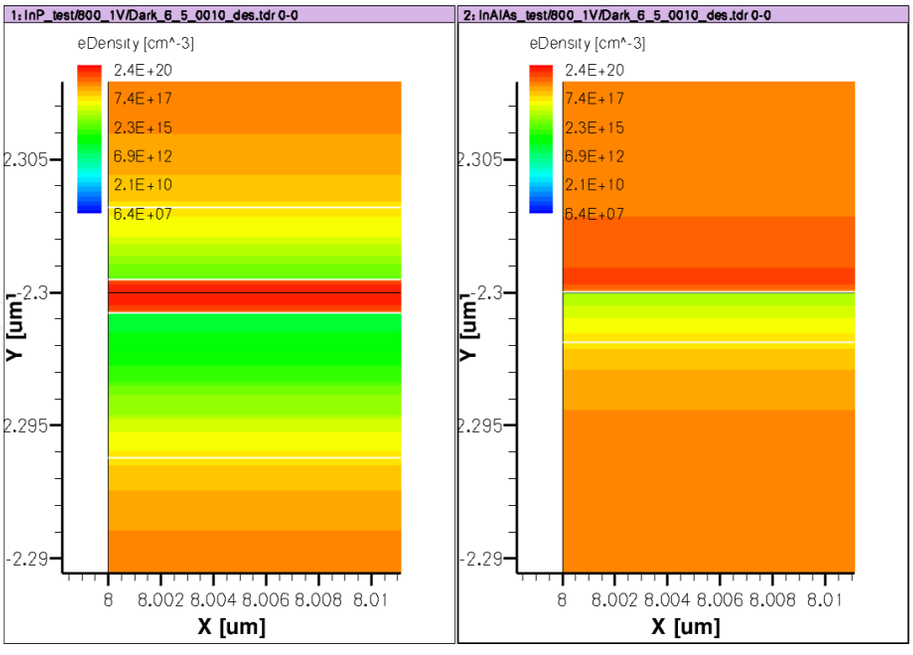


**Figure 4.** Comparison of the electron concentration in the InP/InGaAs contact layer $n^{++}/N^{++}$isotype heterojunction (left) with that in the theInAlAs/InGaAs contact layer $n^{++}/N^{++}$isotype heterojunction (right). The black line at 2.3 μm designates the metalurgical boundary between the $n^{++}$InGaAs layer (top in the figure) and the wider bandgap $N^{++}$ layer.

A photodetector's noise current is proportional to its dark current. Therefore, the InP based SG-OEM should have better noise performance. The I-V curves in Figure 3 also show that the InP/ $In_{0.53}Ga_{0.47}As$ based structure is less susceptible to the Early effect and punch-through breakdown. This is illustrated by the fact that the InP/ $In_{0.53}Ga_{0.47}As$ based structure has a flatter current curve and does not have the sudden current increase of the $In_{0.52}Al_{0.48}As$/ $In_{0.53}Ga_{0.47}As$ based structure at 4.5 V, which is due to the device approaching punch-through breakdown as the base width decreases with the Early effect.

### 3.2. Base – Emitter/Collector Interface Layers

Our prior work on InAlAs/InGaAs SG-OEMs predicted that using a highly doped interface layer in InAlAs based devices would improve their performance [20,21]. This phenomenon was investigated for InP based devices as well. Figure 5 shows two nearly identical device structures, where the only difference is the presence or absence of the said highly doped interface layers. The structure InP_A has the interface layers while structure InP_B does not.Figure 6 shows the predicted performance of the two structures.

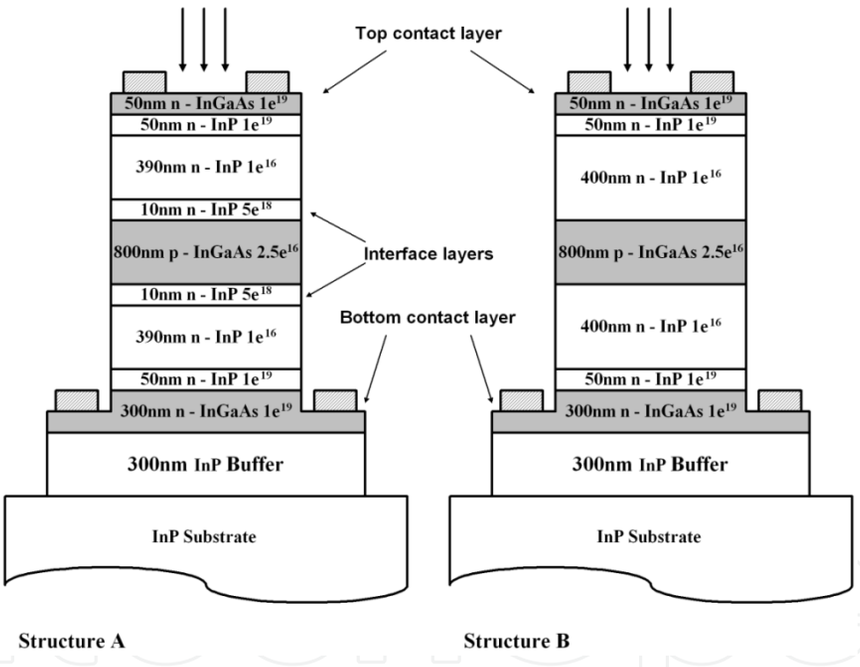


**Figure 5.** Schematic of the InP / $In_{0.53}Ga_{0.47}As$ heterostructure based symmetric gain optoelectronic mixers for investigating the effect of base-emitter interface layers. Structure InP_A has the interface layers while structure InP_B does not.

Structure InP_B, without the interface layer, is predicted to have a larger optical current than structure InP_A at low bias voltages. Figure 6 also shows that structure B is less susceptible to the Early effect, and has lower dark current. The larger optical current and the lower dark current of structure InP_B is due to structure InP_B having a larger effective base thickness than structure InP_A. In structure InP_A, the highly doped (10 nm, $10^{18}$ $cm^{-3}$) emitter interface layers force practically all of the depletion region to extend into the base. The emit-

http://dx.doi.org/10.5772/51461

ter/collector layers of structure InP_B are doped slightly lower than the base layer, therefore most of the depletion region extends into these layers instead of the base. Thus, the InP_B device has a larger effective base width, which increases the optical current by allowing more electron-hole pairs to be generated, and decreases the dark current by inducing more recombination at the base.

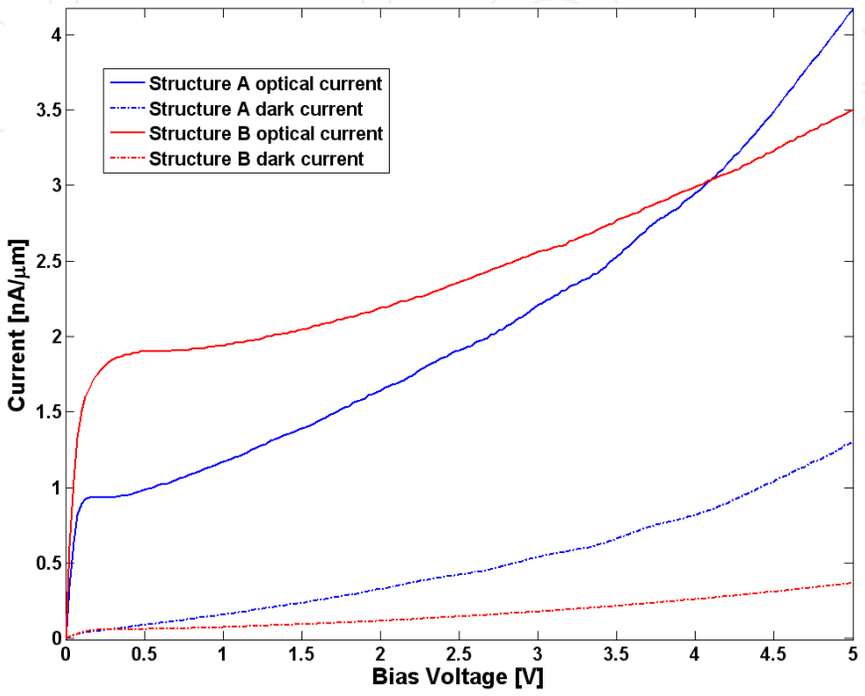


**Figure 6.** Dark and optical currents versus bias voltage for two InP/ $In_{0.53}Ga_{0.47}As$ based symmetric gain optoelectronic mixers with the same layer thickness and doping. Structure InP_A (with the interface layer) and structure InP_B (without the inter face layer).

Figure 7 shows the responsivity versus the bias voltage for structure InP_A and structure InP_B. Structure InP_B is predicted to have larger responsivity than structure InP_A throughout the bias range. This agrees reasonably well with the dark and optical currents plotted in Figure 6, as the responsivity is directly proportional to the difference of optical and dark currents. Structure B has a responsivity of 12.95 A/W at 2 V. This value is about 1.5 times of the one of structure A, which is 8.194 A/W at 2 V. The currents and responsivity plots displayed above illustrate the fact that structure B (without the interface layers) is a better candidate for the symmetric gain optoelectronic mixer design.

SG-OEM structures with base widths ranging from 500 nm to 1 μm were simulated with and without the highly doped interface layers. Structure A devices, with the interface layers, are more susceptible to punch-through breakdown, as can be seen from their dark current characteristics shown in Figure 8. In contrast, the structure B devices were better behaved, as shown in Figure 9. The highly doped emitter/base interface layer in the Structure A devices forces the depletion region to extend mostly into the base layer, resulting in an early punch-through breakdown.

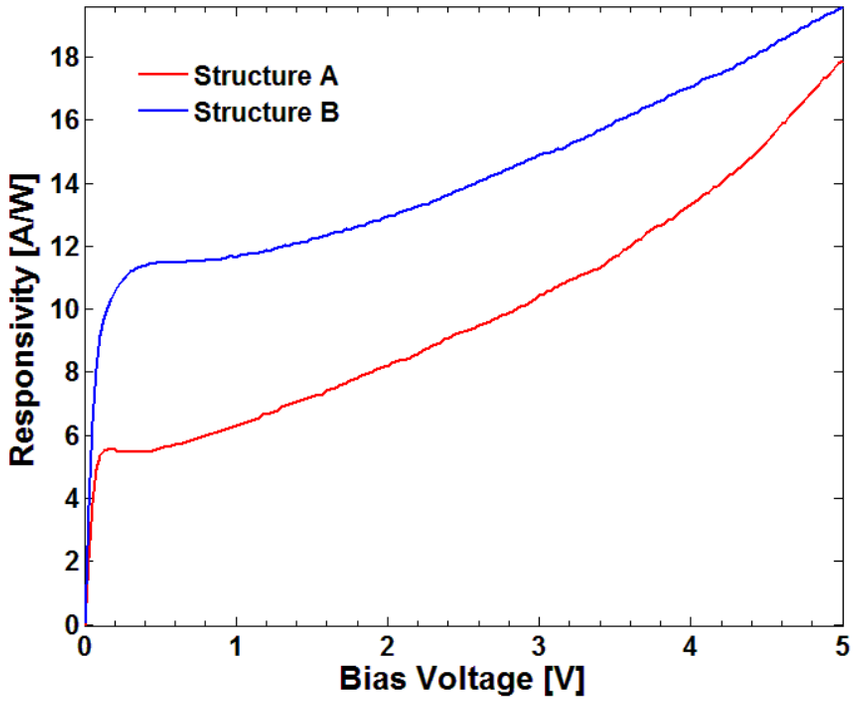


**Figure 7.** Responsivity versus bias voltage for two InP/ In0.53Ga0.47As based symmetric phototransistors with the same layer thickness and doping. Structure InP_A (with the interface layer) and structure InP_B (without the interface layer).

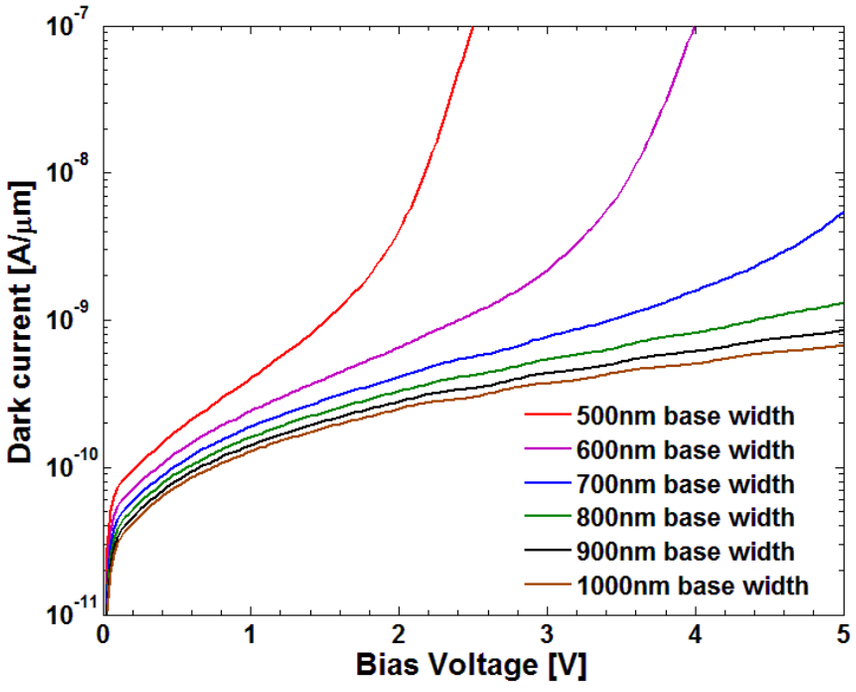


**Figure 8.** Dark current of structure InP_A as a function of base thickness. The base thickness ranges from 500 nm to 1000 nm.

http://dx.doi.org/10.5772/51461

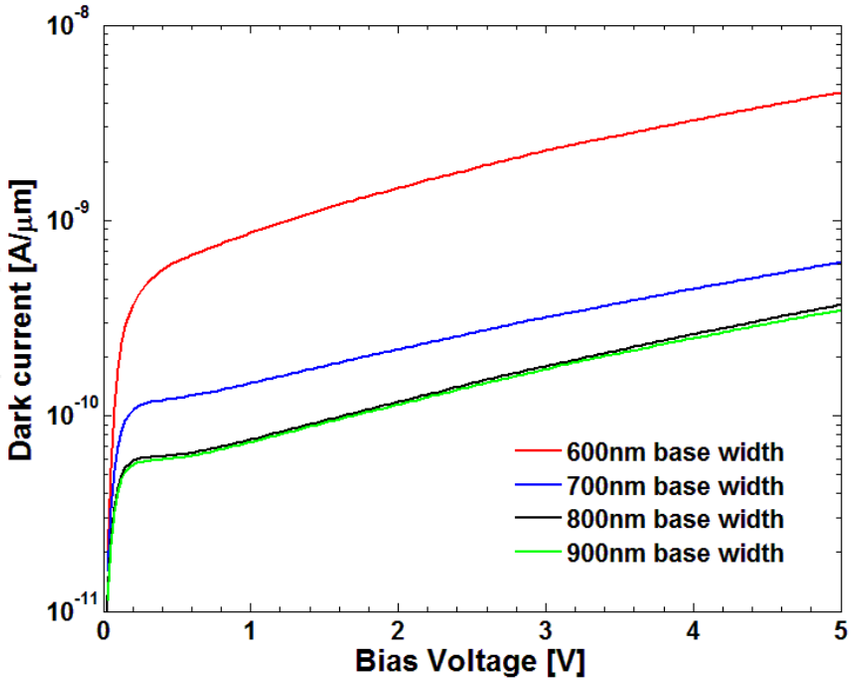


**Figure 9.** Dark current of structure InP_B as a function of the base thickness. The base thickness ranges from 600 nm to 900 nm.

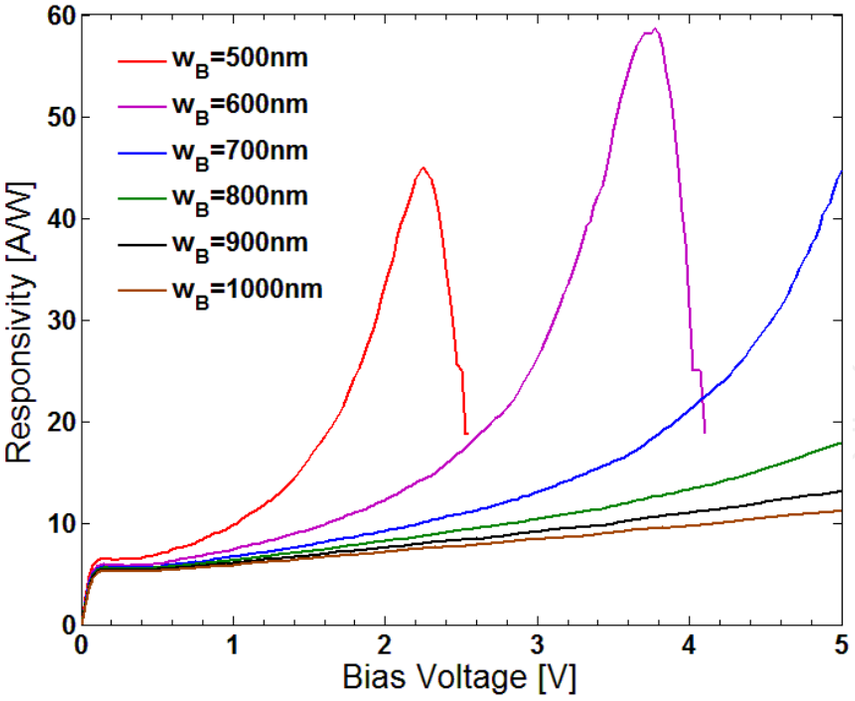


**Figure 10.** Responsivity of structure InP_A as a function of the base thickness. The base thickness ranges from 500 nm to 1000 nm.

The responsivities of the devices were extracted using simulations with an incident light power of 1 mW/cm$^2$, corresponding to an incident optical power of 1.6 nW/μm. Figure 10 shows the DC responsivity of Structure InP_A devices with bases thickness ranging from 500 nm to 1000 nm, with steps of 100 nm. Devices with base thickness below 800 nm show punch-through breakdown effects, where the responsivity increases rapidly as the base narrows, then falls down rapidly when the device punches through.

Figure 11 shows the DC responsivity of four InP/ $In_{0.53}Ga_{0.47}As$ SG-OEMs based on structure InP_B, with base thickness from 600 nm to 900 nm. Similar to structure InP_A devices, the responsivity decreases with increasing base thickness. However, the punch-through behaviour does not occur under 5 V, which agrees with the dark current curves presented in Figure 9.

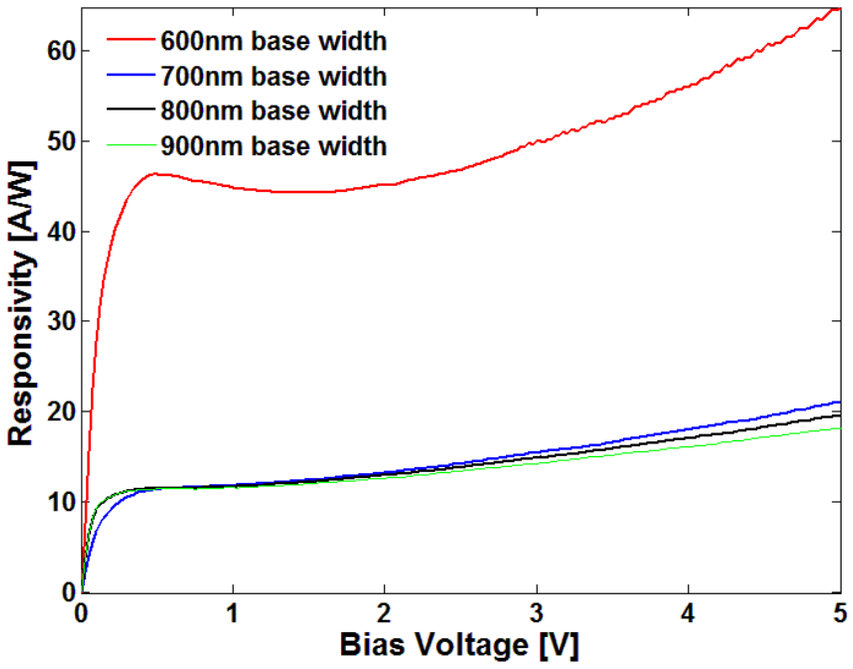


**Figure 11.** Responsivity of structure InP_B as a function of the base thickness. The base thickness ranges from 600 nm to 900 nm.

The doping dependence of the responsivity was investigated using a matrix of emitter/collector and base layer doping densities. The two extremes and the best case scenario are summarized below, in table 5. Doping profile 1 results in rapid punch-through of the SG-OEM. While a traditional homojunction bipolar junction transistor (BJT) has an emitter layer that is heavily doped compared to the base, the wider bandgap of the InP layer compared to InGaAs results in increased injection efficiency. Therefore, the collector / emitter layer doping levels can be reduced in comparison to the base, making doping profiles 2 and 3 practical.

Figure 12 shows responsivity as a function of doping profile for structure B devices,. These devices were simulated for a base width of 800 nm. The device with doping profile 1 exhibits punch-through effects rapidly, reaching its peak responsivity of 81.25 A/W at 3V. The rapid decline in responsivity past 3V is due to punch-through breakdown. The device with

http://dx.doi.org/10.5772/51461

doping profile 3 shows no improvement over the InGaAs MSMs [4,5], having an average responsivity of 0.36 A/W over the bias range. The device with doping profile 2 presents a good compromise for the end application, with responsivities above 10 A/W for most of the bias range. For example, the predicted responsivity at 2V is 12.95 A/W. This represents a factor of 38 improvement over the InGaAs MSMs.

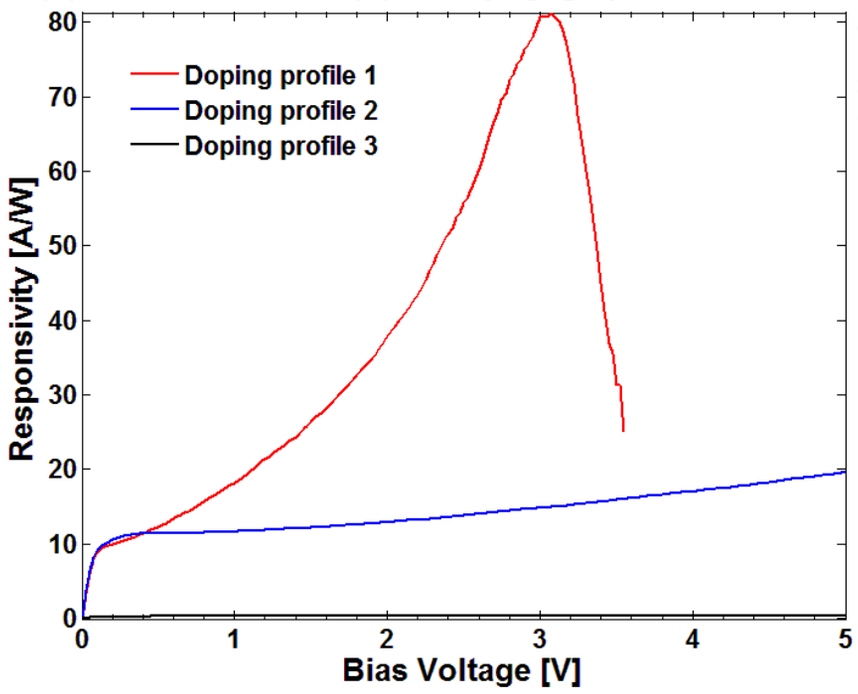


**Figure 12.** Responsivity of structure InP_B as a function of the doping profiles given in table 5. Base thickness is 800 nm.

## 4. Device Model

The equivalent circuit model of the SG-OEM is based on the equivalent circuit model of a heterojunction phototransistor. The equivalent circuit model is shown in Figure 13. This model is based on the conventional hybrid-π model.The resistance $r_T$represents the equivalent series resistance of the top metal-semiconductor contact, the contact layers and the top emitter/collector layer.The resistance $r_B$represents the equivalent series resistance of the bottom metal-semiconductor contact, the contact layers and the bottom emitter/collector layer. $C_\mu$ and $C_\pi$represent the junction diffusion capacitances of the base – emitter and base – collector junctions, respectively.$r_\mu$ and $r_\pi$ are the diffusion resistances of these two junctions. The resistance $r_o$ represents the Early effect. The current source $I_{dark}$ represents the dark current of the optoelectronic mixer. $I_{opt}$ represents the photocurrent due to absorption in the base, which is amplified by transistor action. Photon absorption in the InGaAs contact layers is ignored in this analysis as it is substantially smaller than in the base layer. This model can be used for both DC analysis and AC small signal analysis of the device performance. The

circuit parameters were calculated theoretically and extracted from Sentaurus TCAD two-dimensional simulations.

| | Base Doping | Collector / Emitter Doping |
|---|---|---|
| Profile 1 | $1x10^{16}\,cm^{-3}$ | $5x10^{16}\,cm^{-3}$ |
| Profile 2 | $2.5x10^{16}\,cm^{-3}$ | $5x10^{15}cm^{-3}$ |
| Profile 3 | $5x10^{16}\,cm^{-3}$ | $5x10^{15}cm^{-3}$ |

**Table 5.** The base and emitter/ collector doping profiles for the responsivity doping dependence study

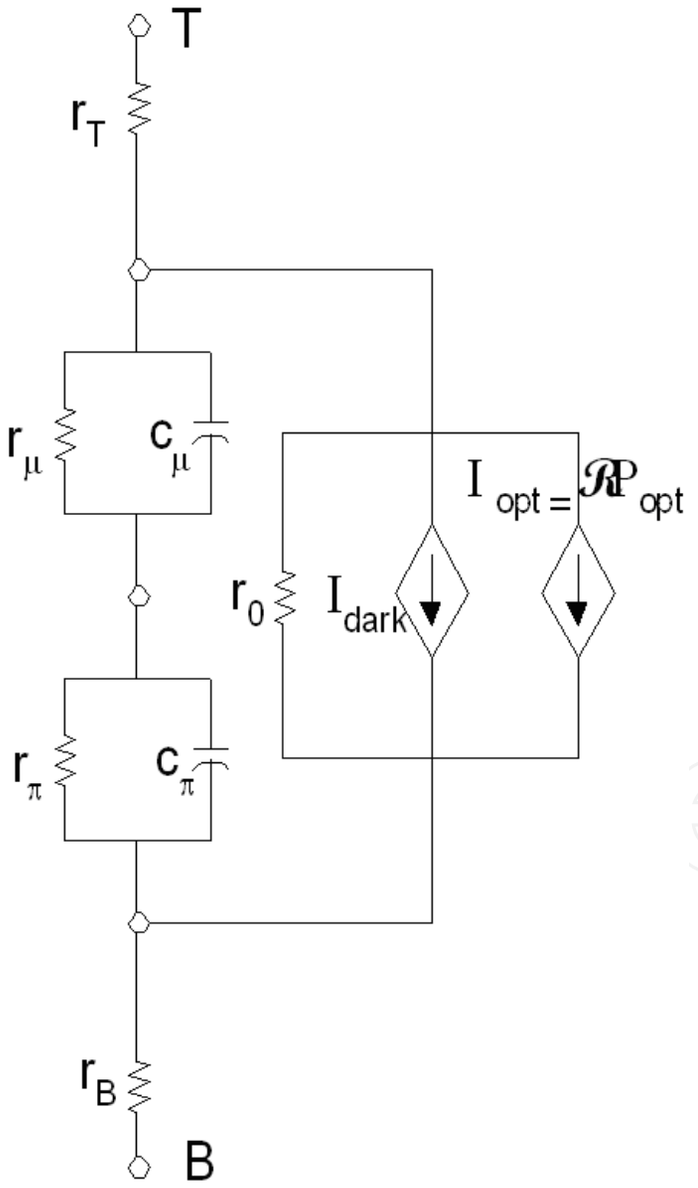


**Figure 13.** (a) Equivalent circuit model of the SG-OEM device structure.

http://dx.doi.org/10.5772/51461

The equivalent resistances $r_T$ and $r_B$ model the metal-semiconductor junction, the degenerately doped InP and InGaAs contact layers, the isotype heterojunction between these contact layers and the quasi-neutral regions (QNRs) of the emitter and collector. Of these components, the quasi-neutral region resistance and the isotype heterojunction dominate $r_T$ and $r_B$. The resistance of the contact layers and the quasi-neutral region can be predicted by using the conductivity of the semiconductor layers, and can be formulated as:

$$r = \frac{w_{layer}}{q\mu_n nd}\left[\Omega.\text{cm}\right] \tag{4}$$

where $w_{layer}$ is the layer thickness, d the width of the layer, q elemental charge, n the free electron density, and $\mu_n$ the mobility of electrons in the layer. The unit of the contact resistance as defined by Equation 4 is Ω.cm.

The second contributor to the voltage drop at the contact layers is the highly doped InP/InGaAs isotype heterojunction interface. The carrier conduction at the highly doped InP/InGaAs isotype heterojunction interface can be analyzed based on the band diagram shown in Figure 14. The conduction band edge is similar to that of a rectifying metal – semiconductor contact. Such a contact can have one of three conduction mechanisms: thermionic emission, thermionic-field emission and field emission. It was determined that field emission dominated the current conduction between the InP and InGaAs layers, due to the very high doping densities of both layers.

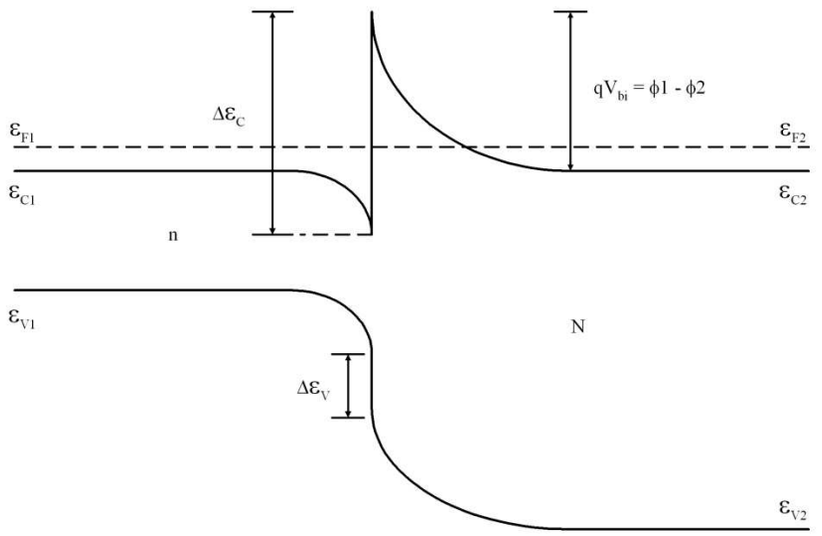


**Figure 14.** Band diagram of the isotype heterojunction formed by the highly doped InP and InGaAs contact layers.

In order to verify the assumptions made above, the contact regions of the original device were modeled seperately in TCAD-Sentaurus and a set of simulations were carried out. The results were then compared with the theoretical calculations. The structures shown in Figure 15 were simulated to verify the calculations for the top and bottom contact resistances. Fig-

ure 16 shows the simulated I-V characteristics for the top and bottom emitter/collector quasi-neutral region and contact layer models depicted in Figure 15. The simulation was done under dark conditions, with the bias voltage being swept from 0 to 5 V.

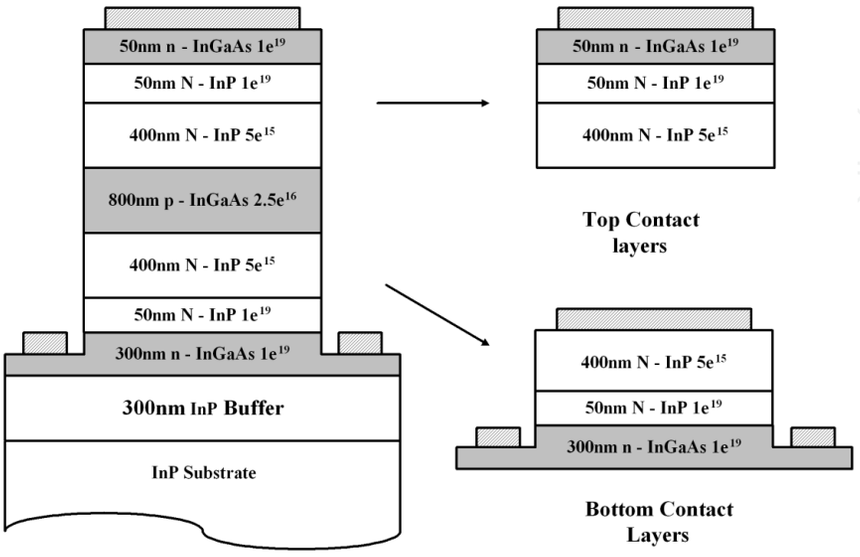


**Figure 15.** Structures for series resistance extraction of InP / $In_{0.53}Ga_{0.47}As$ HPT based SG-OEMs. Original structure is on the left, top contact layers are on the right top and bottom contact layers are on the right bottom.

The dark current of the top emitter/collector region shows a linear trend with increasing bias voltage and the top contact layer series resistance $r_T$ can be calculated from the I-V data presented in Figure 16 using:

$$r_{eq} = \frac{\Delta V}{\Delta I} \tag{5}$$

where $r_{eq}$ is the equivalent resistance ($r_T$ or $r_B$), $\Delta V$ is the voltage difference between two points and the $\Delta I$ is the corresponding current difference on the I-V curve shown in Figure 16.The value of $r_T$, for this structure, is calculated to be $2.97 \times 10^{-2}$ Ω–cm. This value is close to the sum of the theoretically calculated quasi-neutral region resistance ($6.9 \times 10^{-3}$Ω–cm) and isotype heterojunction field emission equivalent resistance($1.03 \times 10^{-2}$Ω–cm). Therefore, it can be concluded that the top contact series resistance is dominated by the quasi-neutral layer resistance and the field emission equivalent resistance of the isotype heterojunction formed by the InGaAs/InP contact layers. The I-V curve of the bottom contact layer, on the other hand, shows a non-linear saturating trend as the voltage increases. The current saturation is induced by the narrowing of the contact layer after the mesa etch step. The increase of the current is limited by the narrow corner region of the InGaAs contact layer. The equivalent resistance is predicted to be approximately 0.57 Ω–cm, assuming the contact layer is etched mid-way and the current starts to crowd in the narrowing contact layer. This resistance will depend on accurate control of the inner mesa etch step in the device fabrication process and can be an issue at high current levels.

http://dx.doi.org/10.5772/51461

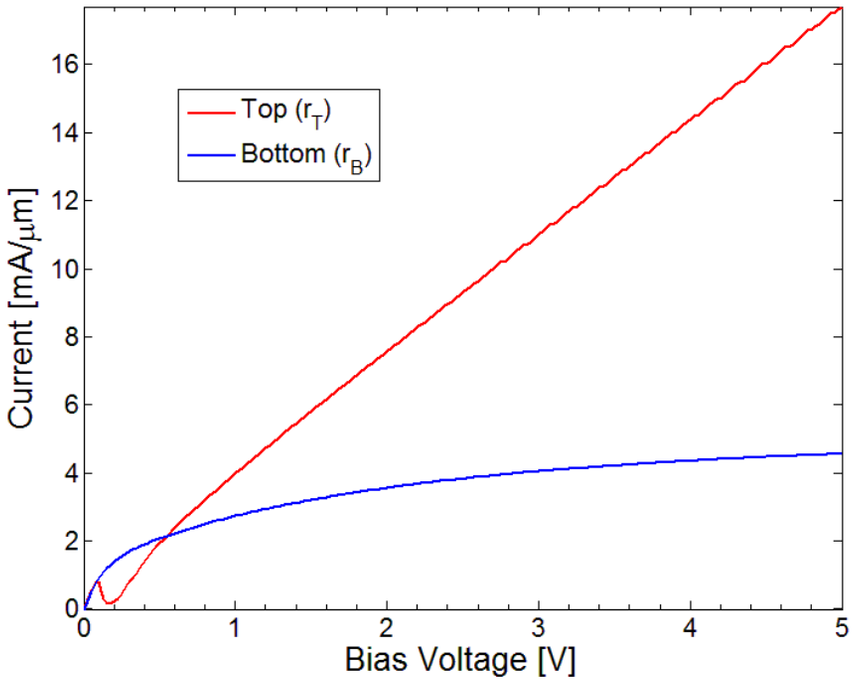


**Figure 16.** Dark current versus bias voltage for top and bottom contact layers of InP / $In_{0.53}Ga_{0.47}As$ HPT based SG-OEMs.

The frequency response related parameters are the junction capacitances $C_\mu$ and $C_\pi$. These can be calculated form the junction capacitance formula for a heterostructure:

$$C = \sqrt{\frac{qN_A N_{Dr,baser,E/C}}{2(N_{Ar,base} + N_{Dr,E/C})(V_{bi} + V_R)}} \tag{6}$$

where $N_A$ and $N_D$ are the doping densities of base and emitter/collector, respectively, $\varepsilon_{r,base}$ is the relative permitivity of the InGaAs base and $\varepsilon_{r,E/C}$ that of the InP emitter/collector, $V_{bi}$ is the built-in barrier, $V_R$is the bias voltage and $q$ is unit charge. The total capacitance of the SG-OEM device is dominated by the junction capacitance of the reverse biased junction.

Equivalent capacitance of the SG-OEM was extracted for both the full structure and a single base-emitter/collector heterojunction, as shown in Figure 17. The device total capacitance is the capacitance seen between the two terminals of the SG-OEM, which includes the two base-emitter/collector junction capacitances in series amd the base transit time.

A set of AC bias simulations were carried out on the two structures displayed in Figure 17. The simulations were set at dark condition and the bias voltage was swept from 0 to 5V. A small signal simulation was applied at each voltage point and the corresponding capacitance was modeled and calculated. The simulated total capacitance of the original structure and the junction capacitance of the base-emitter heterojunction are plotted in Figure 18 as a function of the bias voltage.

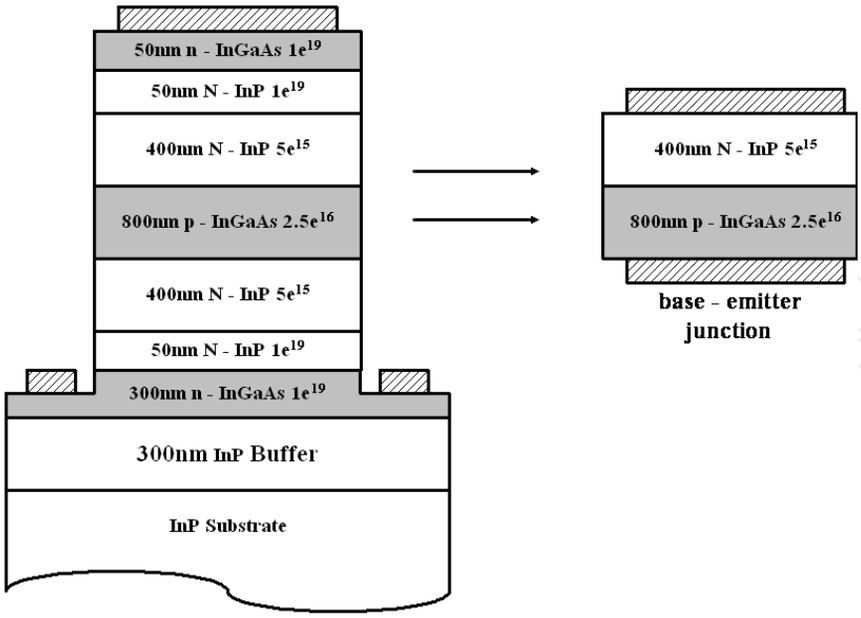


**Figure 17.** Structures used for extracting the equivalent capacitances of InP / $In_{0.53}Ga_{0.47}As$ HPT based SG-OEMs. The full SG-OEM structure is on the left, and a single base-emitter junction is on the right.

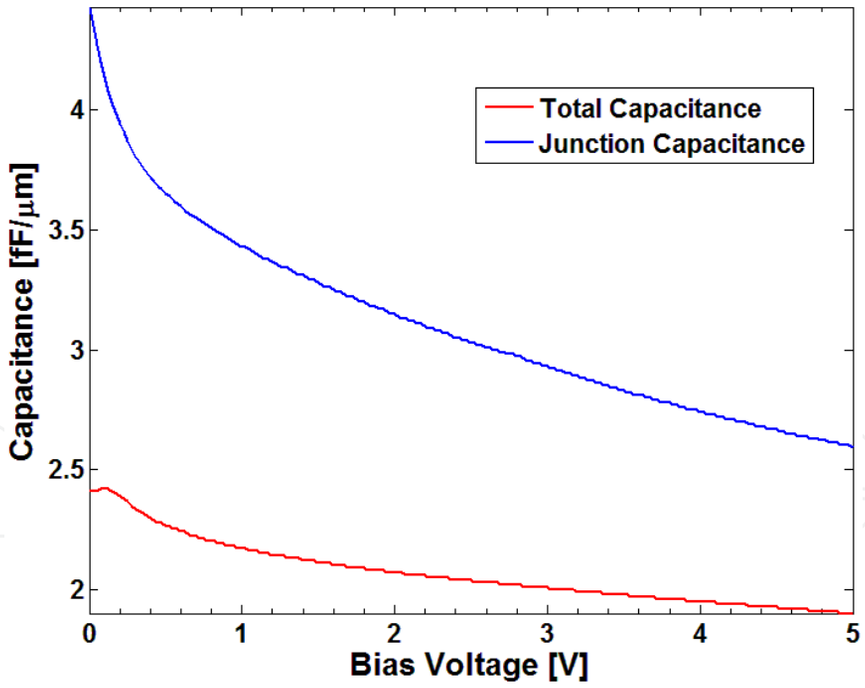


**Figure 18.** Total device capacitance and capacitance of a single reverse-biased base-emitter/ collect junction of InP / $In_{0.53}Ga_{0.47}As$ HPT based SG-OEMs.

A set of AC simulations were carried out on the two structures displayed in Figure 17, with $N_A = 2.5x10^{16}$ $cm^{-3}$ and $N_D = 5x10^{15}$ $cm^{-3}$. The simulations were carried out for dark conditions and the DC bias voltage was swept from 0 to 5V, with a small signal perturbation applied to the bias

http://dx.doi.org/10.5772/51461

voltage. The simulated total capacitance of the SG-OEM structure and that of a single base-emitter/collector heterojunction are plotted in Figure 18 as a function of the bias voltage.

The AC simulation results show that both the device total capacitance and the base-emitter junction capacitance decrease with increasing bias voltage, as would be expected. The capacitance of the reverse biased heterojunction decreases with increasing $V_R$ as given in Equation 6. This is due to the increase of the depletion region width with increasing reverse bias voltage, which leads to a decrease in the junction capacitance. The total capacitance is dominated by the reverse-biased junction capacitance, which has a smaller value than the forward biased junction. At 0V bias, the capacitance of a single heterojunction was calculated to be 4 fF/μm using Equation 6, with $\varepsilon_{r,base} = 13.906$ for the InGaAs layer and $\varepsilon_{r,E/C} = 12.4$ for the InP layer. The TCAD Sentaurus simulation gives 4.434 fF/μm, as shown in Figure 18.At 0V bias, both heterojunction capacitances are equal. Therefore, the equivalent capacitance seen looking into the SG-OEM device, which is the series equivalent capacitance of the two heterojunctions, is half of the capacitance of a single heterojunction.

## 5. Conclusion

Symmetric gain optoelectronic mixers based on InP/ $In_{0.53}Ga_{0.47}As$ heterostructures are promising candidates use in the receivers of chirped-AM LADAR systems. These devices can reduce LADAR system component count and complexity, and improve their performance. Two dimensional device simulations were used to optimize device structure parameters, including base width and doping density, and emitter/collectorlayer doping density. It was determined that highly doped interface layers caused an increase in dark current and device capacitance and also lowered the base punch through breakdown voltage. Therefore, the optimized device design does not contain such an interface layer.

## Acknowledgements

This work was partially supported by the US Army Research Laborayory (Dr. Neal Bambha) under the auspices of the U.S. Army Research Office Scientific Services Program administered by Battelle (Delivery Order 0812, Contract No. W911NF-07-D-0001)

## Author details

Wang Zhang and Nuri W. Emanetoglu*

Electrical and Computer Engineering, University of Maine, Orono, Maine, USA

## References


[1] Jelalian, AV. (1992). Laser Radar Systems. London: Artech House.

[2] Ruff, W., Bruno, J., Kennerly, S., Ritter, K., Shen, P., Stann, B., Stead, M., Sztankay, G., & Tobin, M. (2000). Self-mixing Detector Candidates for an FM/cwLadarArchitecture. *Laser Radar Technology and Applications V*, Proc. SPIE, 4035.

[3] Shen, H., & Aliberti, K. (2002). Theoretical analysis of an anisotropic metal-semiconductor-metal optoelectronic mixer. *Journal of Applied Physics*, 91(6), 3880-3890.

[4] Shen, H., Aliberti, K., Stann, B., Newman, P. G., Mehandru, R., & Ren, F. (2004). Analysis of InGaAs metal-semiconductor-metal OE mixers. *Physics and Simulation of Optoelectronic Devices XII, Proc. SPIE*, 5349.

[5] Shen, H., Aliberti, K., Stann, B., Newman, P., Mehandru, R., & Ren, F. (2003). Mixing characteristics of InGaAs metal-semiconductor-metal photodetectors with Schottky enhancement layers. *Applied Physics Letters*, 82(22), 3814-3816.

[6] Chandrasekhar, S., Hoppe, M. K., Dentai, A. G., Joyner, C. H., & Qua, G. J. (1991). Demonstration of enhanced performance of an InP/InGaAsheterojunction phototransistor with a base terminal. *IEEE Electron Device Letters*, 12(12), 550-552.

[7] Capasso, F., Tsang, W. T., Bethea, C. G., Hutchinson, A. L., & Levine, B. F. (1983). New graded band-gap picosecond phototransistor. *Applied Physics Letters*, 42(1), 93-95.

[8] Thuret, J., Gonzalez, C., Benchimol, J. L., Riet, M., & Berdaguer, P. (1999). High-speed InP/InGaAsheterojunction phototransistor for millimeter-wave fibre radio communications. *Proc. 11th Int. Conference on Indium Phosphide and Related Materials*, 389-392.

[9] Milano, R. A., Dapkus, P. D., & Stillman, G. E. (1982). An analysis of the performance of heterojunction phototransistors for fiber optic communications. *IEEE Transactions on Electron Devices*, 29(2), 266-274.

[10] Choi, C. S., Seo, J. H., Choi, W. Y., Kamitsuna, H., Ida, M., & Kurishima, K. (2005). GHz Bidirectional Radio-on-Fiber Links Based on InP-InGaAs HPT Optoelectronic Mixers. *IEEE Photonic Technology Letters*, 17(12), 2721-2723.

[11] Polleux, J. L., Paszkiewicz, L., Billabert, A. L., Salset, J., & Rumelhard, C. (2004). Optimization of InP-InGaAs HPT Gain: Design of an Opto-Microwave Monolithic Amplifier. *IEEE Transactions on Microwave Theory and Technology*, 52(3), 871-881.

[12] Leu, L. Y., Gardner, J. T., & Forrest, S. R. (1991). A high-gain high-bandwidth $In_{0.53}Ga_{0.47}As$/InPheterojunction phototransistor for optical communications. *Journal of Applied Physics*, 69(2), 1052-1062.

[13] Liu, , Seeds, A. J., & Wake, D. (1997). Two-terminal edge-coupled InP/InGaAsheterojunction phototransistor optoelectronic mixer. *IEEE Microwave and Guided Wave Letters*, 7(3), 72-74.

[14] Van de Casteele, J., Vilcot, J. P., Gouy, J. P., Mollot, F., & Decoster, D. (1996). Electro-optical mixing in an edge-coupled GaInAs/InPheterojunction phototransistor. *Electronics Letters*, 32(11), 1030-1032.

[15] Chen, C. Y., Cho, A. Y., Garbinski, P. A., Bethea, C. G., & Levine, B. F. (1981). Modulated barrier photodiode: A new majority-carrier photodetector. *Applied Physics Letters*, 39(4), 340-342.

[16] Chen, CY. (1981). Theory of a modulated barrier photodiode. *Applied Physics Letters*, 39(12), 979-981.

[17] Bethea, C. G., Chen, C. Y., Cho, A. Y., & Garbinski, P. A. (1982). Opto-electronic picosecond sampling system utilizing a modulated barrier photodiode. *Applied Physics Letters*, 40(7), 591-594.

[18] Li, W. Q., & Bhattacharya, P. K. (1989). Integration of a modulated barrier photodiode with a doped-channel quasi-MISFET. *IEEE Electron Device Letters*, 10(9), 415-416.

[19] Qasaimeh, O, Zhou, WD, Bhattacharya, P, Huffaker, D, & Deppe, DG. (2000). Monolithically integrated low-power phototransceiver incorporating InGaAs/GaAs quantum-dot microcavity LED and modulated barrier photodiode. *Electronics Letters*, 36(23), 1955-1957.

[20] Emanetoglu, N. W., Drew, S., Bambha, N., & Bickford, J. R. (2008). Symmetric Gain Optoelectronic Mixers for LADAR. *Proceedings of the 2008 US Army Science Conference*, NP-11.

[21] Drew, S. (2009). Symmetric Gain Optoelectronic Mixers for LADAR Applications. *MS thesis. University of Maine Orono*.

[22] Zhang, W., Emanetoglu, N. W., Bambha, N., & Bickford, J. R. (2010). Design and Analysis of $In_{0.53}Ga_{0.47}As$/InP Symmetric Gain Optoelectronic Mixers. *Solid State Electronics*, 54(12), 1549-1553.

[23] Zhang, W. (2010). InP/$In_{0.52}Ga_{0.47}As$ Symmetric Gain Optoelectronic Mixers for LADAR Applications. *MS thesis. University of Maine Orono*.

IntechOpen